

# Three-Stream Convolutional Networks for Video-based Person Re-Identification

Zeng Yu<sup>1,3</sup>, Tianrui Li<sup>1</sup>, Ning Yu<sup>2</sup>, Xun Gong<sup>1</sup>, Ke Chen<sup>1</sup>, and Yi Pan<sup>3</sup>

<sup>1</sup>School of Information Science and Technology, Southwest Jiaotong University

<sup>2</sup>Department of Computing Sciences, The College at Brockport State University of New York

<sup>3</sup>Department of Computer Science, Georgia State University

## Abstract

*This paper aims to develop a new architecture that can make full use of the feature maps of convolutional networks. To this end, we study a number of methods for video-based person re-identification and make the following findings: 1) Max-pooling only focuses on the maximum value of a receptive field, wasting a lot of information. 2) Networks with different streams even including the one with the worst performance work better than networks with same streams, where each one has the best performance alone. 3) A full connection layer at the end of convolutional networks is not necessary. Based on these studies, we propose a new convolutional architecture termed Three-Stream Convolutional Networks (TSCN). It first uses different streams to learn different aspects of feature maps for attentive spatio-temporal fusion of video, and then merges them together to study some union features. To further utilize the feature maps, two architectures are designed by using the strategies of multi-scale and upsampling. Comparative experiments on iLIDS-VID, PRID-2011 and MARS datasets illustrate that the proposed architectures are significantly better for feature extraction than the state-of-the-art models.*

## 1. Introduction

The re-identification problem aims to identify the same person when he/she moves between non-overlapping cameras distributed at different locations [4]. It has received an increasing attention due to its potential applications such as people tracking in the surveillance videos and criminal investigation. However, it is still a very challenging task because person images/videos captured from the same/different cameras usually have large variations of lighting conditions, viewing points, body poses and backgrounds.

Currently, a variety of person re-identification algorithms have been developed. They can mainly be classified into two categories: still image-based approaches and the video-based ones. However, most of existing methods solve the person re-identification task with the former category [1, 19, 28, 31, 33, 32], while only a few methods are designed with the latter one. In reality, the video-based method is a more natural way to address the task of person re-identification. Intuitively, temporal information appeared in the videos can be used to capture the person motion. Moreover, videos contain rich samples of a person's appearance [15, 14], which allow to build a better model with more discriminative poses, viewpoints, and backgrounds. Therefore, in this paper, we will focus on the problem of video-based person re-identification.

In a video-based method, optical flows are applied to extract temporal information from the consecutive frames of a person. With the extracted optical flows, single-stream and two-stream architectures have been explored. A single-stream architecture concatenates optical flows with RGB images as the inputs of a RNN (or CNN-RNN) model for training the model [24, 35, 37]. For a two-stream architecture, it separately builds two CNN architectures with optical flows and RGB images as their inputs, and then fuses/feeds them to a RNN model [3, 27, 20]. As a result, all the single-stream and two-stream architectures can be viewed as methods of data fusion and model fusion, respectively. Instead of designing approaches for data fusion or model fusion, in this paper we will consider how to design effective architectures of networks that can fully utilize the learned feature maps.

Generally, the operation of pooling is used for downsampling in a CNN architecture. In practice, convolutional layers that have a stride of 2 also perform downsampling directly [6]. It has been shown that max-pooling can achieve reasonable success on the task of video-based person re-

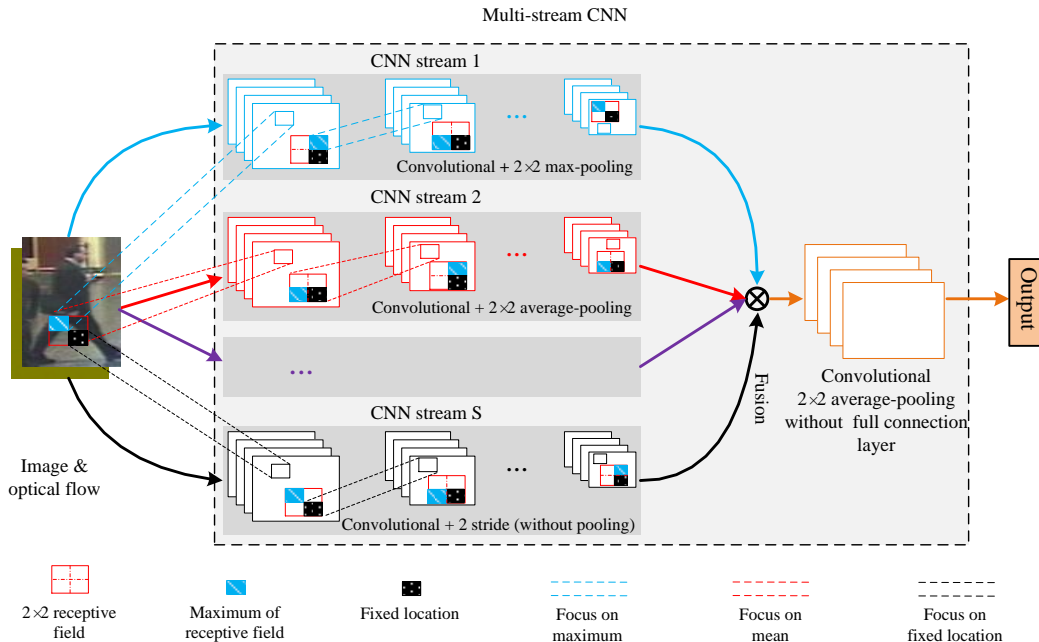


Figure 1. Example of multi-stream convolutional neural network. Different streams learn different aspects of the feature maps. Max-pooling, average-pooling and 2 stride convolutional layer focus on the maximum value, average value and fixed location of receptive field respectively.

identification [24, 35, 37]. However, when we use the max-pooling to sample the feature maps, it will dissipate many learned features. In fact, features that are not the maximum values also can help to solve the problem of person re-identification as shown in Section 4.2.1. In addition, the strategies of multi-scale and upsampling are also beneficial for reusing the learned features via mapping the features into different dimensionalities. Therefore, to make full use of the learned feature maps, we propose three new deep learning models that take the advantages of downsampling, multi-scale and upsampling. In each model, it contains multi-stream CNN architectures, where every stream focuses on different aspects of the learned feature maps.

Fig. 1 illustrates an example of multi-stream CNN architecture. As shown in this figure, we use different strategies to make the proposed model concentrate on different aspects of feature maps (e.g. max-pooling concentrates on the maximum value of receptive field). With these strategies, all the learned features will be fully used for feature representation on the task of video-based person re-identification. Because the best results are obtained by utilizing a three-stream CNN architecture, we refer it as three-stream convolutional network.

The rest of this paper is organized as follows. In Section 2, we will introduce the related work. Section 3 will investigate the properties of different combinations, and then present the novel architectures. Section 4 will compare

the performance of proposed method with other relevant state-of-the-art algorithms on iLIDS-VID, PRID-2011 and MARS datasets. Conclusions together with some further studies are summarized in the last section.

## 2. Related Work

In the past few years, researchers have designed various algorithms for person re-identification. These algorithms mainly focus on two aspects: feature representations [23, 18, 40] and metric learning [17, 34, 38, 39, 25]. Gray and Tao [5] learned viewpoint invariant features for pedestrian recognition by combining spatial and color information. Farenzena et al. [2] extracted the texture histograms by studying the perceptual principles of symmetry and asymmetry. Kviatkovsky et al. [12] proposed a novel intradistribution structure based on the color distributions, which can learn the illumination invariant features under a variety of imaging conditions. Weinberger et al. [30] adopted the idea of large margin nearest neighbor metric (LMNN) to gather the  $k$ -nearest neighbors and separate examples from different classes by a large margin. Zheng et al. [42] utilized relative distance comparison (RDC) to maximize the likelihood of a pair of true matches. Liao et al. [16] employed an effective architecture called Local Maximal Occurrence (LOMO) to learn a stable representation against viewpoint changes by maximizing the occurrence.

To use the temporal information, more and more

researchers began to consider the video-based re-identification problem. With HOG3D descriptor, Klaser et al. [11] calculated the highest similarity between two video fragments as the distance of these two videos. Karaman et al. [8] attempted to make the similar frames to have the similar labels by using a conditional random field (CRF). Yan et al. [36] tried to use the recurrent feature aggregation network (RFA-Net) to aggregate sequence level representations with LSTM. More recently, McLaughlin et al. [24] applied a CNN to obtain the image-level representation and then fed it into a RNN to exploit the temporal information. Zhang et al. [37] replaced the RNN with bidirectional recurrent neural networks (BRNN) to effectively learn spatio-temporal features. Zhou et al. [43] employed the spatial recurrent model (SRM) and temporal attention model (TAM) to study the spatio-temporal information. Xu et al. [31] utilized spatial pyramid pooling and attentive temporal pooling to improve the performance. Liu et al. [20] tried to accumulate the motion context by using a two-stream convolutional architecture. Unlike the existing deep learning based methods for video-based re-identification, our proposed models use a multi-stream convolutional architecture, in which different streams learn different aspects of feature maps and then they merge together to obtain some union characteristics.

### 3. Approach

A recurrent-convolutional network for video-based person re-identification usually consists of CNN architectures and a RNN network. The CNN architectures are utilized to extract feature representation from the multiple frames of video. The RNN network is applied to learn the temporal information between them. Downsampling is essential to a CNN architecture. As discussed previously, the traditional downsampling operation such as max-pooling only uses the maximum value, ignoring a lot of learned features. Therefore, in this paper, we propose the multi-stream convolutional network for video-based person re-identification. It can make full use of the learned feature maps by employing different streams of convolutional network which focus on different properties of the feature maps. To further reuse the learned features, two multi-scale convolutional networks are also developed.

#### 3.1. Different multi-streams

In this part, we consider two questions: 1) How to generate different multi-streams? 2) How to make different multi-streams focus on different aspects of the learned feature maps? The operation of max-pooling only focuses on the maximum value, wasting a lot of information. For example, if we use a  $2 \times 2$  max-pooling, only a quarter of the learned feature maps are adopted. Although the average-pooling considers all the feature maps, it treats all the fea-

tures equally. Fortunately, a convolutional layer with a stride greater than 2 also performs downsampling by replacing the pooling operation. It concentrates on the learned feature maps with fixed positions. The dilated max/average-pooling also can be used for downsampling. With dilated max/average-pooling, the networks focus on larger receptive field. Recently, many pooling operations such as adaptive max/average-pooling and fractional max-pooling have been proposed. With these pooling operations, we can build multi-stream convolutional networks. Because different multi-streams focus on different aspects of the learned feature maps (e.g. max-pooling concentrates on the maximum value of receptive field), we can make full use of feature maps with these multi-streams. In fact, we can also generate different streams by using an ‘‘upconvolutional’’ layer, multi-scale or upsampling achieved by padding the smaller map with zeros. In the experiments, we will investigate most of the generating methods coupled with various of convolutional networks.

As shown in Section 4.2.1, networks with different streams even including the one with the worst performance work better than networks with same streams, where each one has the best performance alone. It means that a stream with the poor performance can further improve the performance of the one with good result. In other words, different streams complement each other to learn some different aspects of the feature maps, that they can not learned independently. As a result, in our proposed model, three different streams will complement each other to learn some union features.

#### 3.2. Spatial fusion with multi-stream networks

We consider different methods for fusing multi-stream convolutional networks. Because each network in the multi-streams concentrates on an aspect of the learned feature maps and it has the same channels and spatial resolution at the layers to be fused, we can simply stack layers on one network. To make it more concrete, we study several ways of fusing layers among multi-stream networks. We use  $\mathbf{x}^s \in \mathbb{R}^{H \times W \times D}$  to denote the feature maps of the  $s$ -th ( $s = 1, 2, \dots, S$ ) stream, where  $S$ ,  $W$ ,  $H$  and  $D$  are the number of multi-streams, the width, height and channel number of the feature maps. Let  $f$  be the fusion function:  $f(\mathbf{x}^1, \mathbf{x}^2, \dots, \mathbf{x}^S) \rightarrow \mathbf{y}$ , where  $\mathbf{y}$  is the fused feature map.  $f$  can be easily used in any layer of the multi-streams if they have the same channels and spatial resolution.

- **Sum fusion.** In a multi-stream network, the sum fusion,  $\mathbf{y}^{sum} = f^{sum}(\mathbf{x}^1, \mathbf{x}^2, \dots, \mathbf{x}^{S_1})$ , is to compute the sum of some or all the feature maps at the same spatial locations  $i, j$  and channels  $d$ :

$$y_{i,j,d}^{sum} = x_{i,j,d}^1 + x_{i,j,d}^2 + \dots + x_{i,j,d}^{S_1}, \quad (1)$$

where  $1 \leq i \leq H, 1 \leq j \leq W, 1 \leq d \leq D, 2 \leq S_1 \leq S$  and  $\mathbf{x}^1, \mathbf{x}^2, \dots, \mathbf{x}^{S_1}, \mathbf{y}^{sum} \in \mathfrak{R}^{H \times W \times D}$ .

- **Max fusion.** Similarly, the max fusion,  $\mathbf{y}^{max} = f^{max}(\mathbf{x}^1, \mathbf{x}^2, \dots, \mathbf{x}^{S_1})$ , takes the maximum of some or all the feature maps:

$$y_{i,j,d}^{max} = \max\{x_{i,j,d}^1, x_{i,j,d}^2, \dots, x_{i,j,d}^{S_1}\}, \quad (2)$$

- **Channel fusion.** In a multi-stream network, the channel fusion,  $\mathbf{y}^{cha} = f^{cha}(\mathbf{x}^1, \mathbf{x}^2, \dots, \mathbf{x}^{S_1})$ , stacks some or all the feature maps at the same spatial locations  $i, j$  across channels  $d$ :

$$y_{i,j,t}^{cha} = x_{i,j,d}^s, \quad (3)$$

$$s.t \quad \begin{cases} s = 1, & 1 \leq t \leq D \\ s = 2, & D + 1 \leq t \leq 2D \\ \dots \\ s = S_1, & (S_1 - 1) \times D + 1 \leq t \leq S_1 \times D \end{cases}$$

where  $\mathbf{y}^{cha} \in \mathfrak{R}^{H \times W \times (S_1 \times D)}$ .

- **Width fusion.** In a multi-stream network, the width fusion,  $\mathbf{y}^{wid} = f^{wid}(\mathbf{x}^1, \mathbf{x}^2, \dots, \mathbf{x}^{S_1})$ , stacks some or all the feature maps at the same spatial heights  $i$  and channels  $d$  across spatial widths  $j$ :

$$y_{i,t,d}^{wid} = x_{i,j,d}^s, \quad (4)$$

$$s.t \quad \begin{cases} s = 1, & 1 \leq t \leq W \\ s = 2, & W + 1 \leq t \leq 2W \\ \dots \\ s = S_1, & (S_1 - 1) \times W + 1 \leq t \leq S_1 \times W \end{cases}$$

where  $\mathbf{y}^{wid} \in \mathfrak{R}^{H \times (S_1 \times W) \times D}$ .

- **Height fusion.** In a multi-stream network, the height fusion,  $\mathbf{y}^{hig} = f^{hig}(\mathbf{x}^1, \mathbf{x}^2, \dots, \mathbf{x}^{S_1})$ , stacks some or all the feature maps at the same spatial widths  $j$  and channels  $d$  across spatial heights  $i$ :

$$y_{t,j,d}^{hig} = x_{i,j,d}^s, \quad (5)$$

$$s.t \quad \begin{cases} s = 1, & 1 \leq t \leq H \\ s = 2, & H + 1 \leq t \leq 2H \\ \dots \\ s = S_1, & (S_1 - 1) \times H + 1 \leq t \leq S_1 \times H \end{cases}$$

where  $\mathbf{y}^{hig} \in \mathfrak{R}^{(S_1 \times H) \times W \times D}$ .

With the baseline model as shown in Fig. 2, we evaluate and compare each possible fusion method in terms of their classification accuracy in our experiments. Note that the number of channel is arbitrary for channel fusion. We can change the number of channel on any stream and optimize

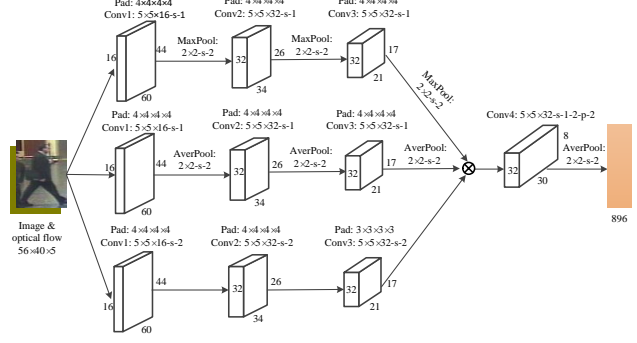


Figure 2. The architecture of three-stream convolutional network. The inputs consist of RGB images and optical flows. We use it as the baseline model for choosing parameters.

over the filters at any layer to make this arbitrary correspondence useful for subsequent learning. In the case of width fusion, the width number of the feature maps can also be changed. Similarly to width fusion, the height number of the feature maps is again arbitrary for height fusion. For convenience, we fix the width, height and channel number of the feature maps for all the layers to be fused in the experiments.

Spatial fusion can be applied at any point among the multi-stream networks when they have same spatial resolution. Actually, the spatial fusion have significant impact on the number of parameters and layers. In the experimental section, we evaluate some networks that spatial fusion can be placed at different points to implement e.g. early-fusion or late-fusion.

In this paper, we show that it is not necessary to use a full connection layer in the multi-stream convolutional networks, even it's harmful in a recurrent-convolutional network. Many previous work have been shown that a full connection layer with small size of 128 is necessary at the end of convolutional networks and it can achieve the state-of-the-art performance. However, in the multi-stream networks, we replace the full connection layer with a convolutional layer. As a result, the image-level representation is more meaningful and the dimension of feature space can be set to a very high value reserved more information of the image. Without a full connection layer at the end of convolutional networks, we obtain the state-of-the-art performance.

### 3.3. Multi-stream with multi-scale and upsampling

As mentioned above, we can easily implement spatial fusion at any point among the multi-stream networks, with the only constraint that the feature maps have the same spatial resolution. This can be achieved by using multi-scale, upsampling or an "upconvolutional" layer. Multi-scale can be applied to mapping the features into different dimensional-

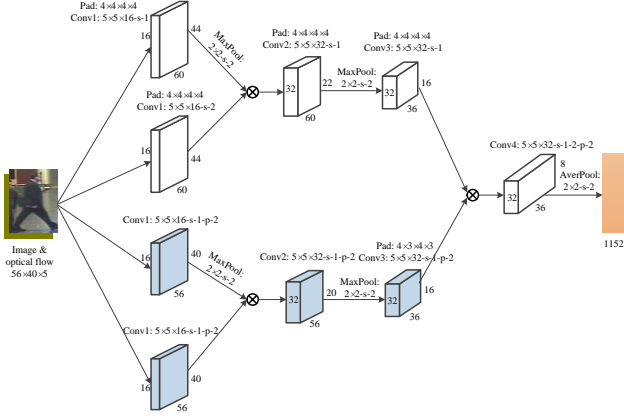


Figure 3. The architecture of two-stream multi-scale convolutional network. It has 3 width fusion layers.

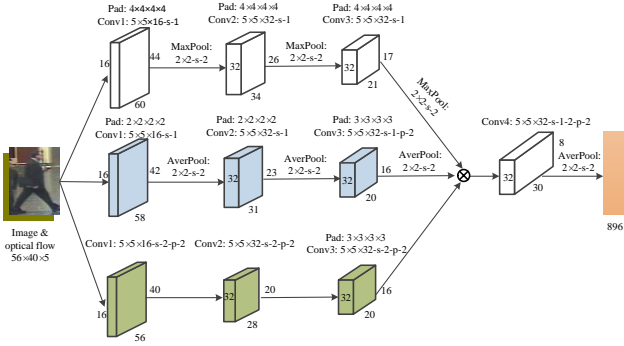


Figure 4. The architecture of three-stream multi-scale convolutional network.

ities. Upsampling can simply be implemented by padding the smaller feature map with zeros. However, we do not utilize the “upconvolutional” layer in our models. In practice, multi-scale and upsampling are adaptive to variations in person/body size due to perspective effect or image resolution in the frames of the video.

With multi-scale and upsampling, we construct two multi-stream CNN architectures: two-stream multi-scale network and three-stream multi-scale network. Similarly to pooling operations, networks with multi-scale focus on some different characteristics of the feature maps. As shown in Fig. 3, the two-stream multi-scale network can be fused at three layers, which can achieve the goal of pixel-wise registration of the channels from each stream. The three-stream multi-scale network uses multi-scale to obtain different dimensionalities at the lower-level layers and gets the same spatial resolution with upsampling before the fusion (higher-level) layer, see Fig. 4.

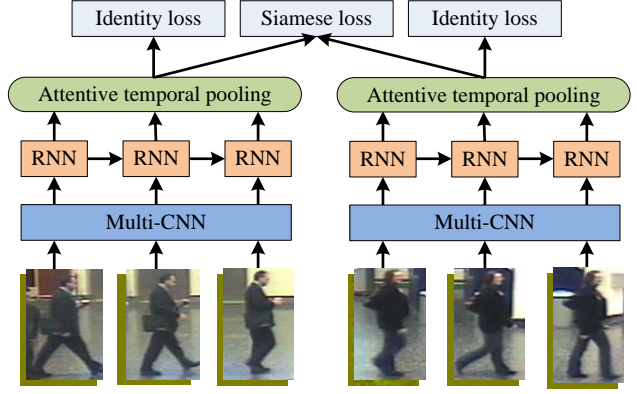


Figure 5. The proposed architecture for video-based person re-identification.

### 3.4. Proposed architecture

Based on the previous discussion, we propose a new attentive spatio-temporal fusion architecture. In fact, it can be extended to three new attentive spatio-temporal fusion models by replacing the part of multi-stream CNN with three effective CNN architectures shown in Figs. 2-4. The choices of the parameters for proposed architectures (e.g. number of stream, spatial fusion method, layer and attentive temporal pooling) are based on our empirical evaluation.

Fig. 5 illustrates the architecture of the proposed network. It employs a Siamese network architecture, which has two sub-networks with same weights. As shown in this figure, our network architecture consists of three parts: convolutional network, the recurrent network and the attentive temporal pooling layer. The recurrent network is used for capturing temporal information of the frames in a video and the attentive temporal pooling layer inspired by the works of [35] guides for effectively extracting this temporal information. For convolutional network, it is a critical part of the attentive spatio-temporal fusion architectures. We design three multi-stream convolutional networks to replace the single-stream or two-stream architectures. As mentioned above, the multi-stream convolutional networks can make full use of the feature maps because each stream focuses on some characteristics of the feature maps.

As suggested by [24], both the Siamese loss and the identity loss are used to train the proposed architectures. Given a pair of sequences of persons  $i$  and  $j$ , we use the Siamese network to obtain the sequence feature vectors  $v_i$  and  $v_j$ . After that, the Siamese loss objective function with Euclidean distance can be given as follows:

$$E(v_i, v_j) = \begin{cases} \|v_i - v_j\|_2^2, & i = j \\ \max\{0, m - \|v_i - v_j\|_2\}, & i \neq j \end{cases} \quad (6)$$

where  $m$  is the margin that separates features of different persons. In addition, we use standard softmax function to



predict the identity of the person in the sequence, and then we adopt the cross-entropy loss to obtain the identity loss objective function  $L(v_i)$  and  $L(v_j)$ . Finally, we define the overall training objective function  $P(v_i, v_j)$  by simultaneously optimizing the Siamese loss and the identity loss:

$$P(v_i, v_j) = E(v_i, v_j) + L(v_i) + L(v_j) \quad (7)$$

Here, we treat the Siamese loss and the identity loss equally. The proposed architectures can be trained end-to-end using back-propagation-through-time. We detail the training parameters in the next section.

## 4. Experimental Results

In this section, we evaluate our proposed models for video-based person re-identification on iLIDS-VID [29], PRID-2011 [7] and MARS [41] datasets and compare the performance with state-of-the-art algorithms. Several important parameters will also be experimentally evaluated.

### 4.1. Datasets

The iLIDS-VID dataset contains 300 persons, where each person is represented by two sequences appeared in two non-overlapping camera views at an airport arrival hall under a multi-camera CCTV network. The length of sequences range from 23 to 192 frames with an average length of 73. Due to clothing similarities for different persons, lighting and viewpoint variations, cluttered background and random occlusions, it becomes very challenging.

The PRID-2011 dataset consists of 749 persons captured by two non-overlapping cameras. Each image sequence has the length of frame from 5 to 675, with an average number of 100. Compared with the iLIDS-VID dataset, it has simple backgrounds and rare occlusions. Following the protocol used in [35], only the first 200 persons captured by both cameras are utilized.

The MARS dataset is the largest video-based person re-identification benchmark dataset to date. It has 1261 different persons, each person has at least two image sequences automatically obtained by DPM detector and GMMCP tracker. These sequences are captured by 2-6 cameras and each identity has 13.2 sequences on average. Similar to the protocol used in [35], we randomly choose two cameras of the same person for evaluation, where the case was reduced to experiences with iLIDS-VID and PRID-2011.

Following [35], we randomly split each dataset into training set and testing set with equal size. We repeat the experiments 10 times with different splits and report the average results with Cumulative Matching Characteristics (CMC) curves. To train the Siamese network, we set the margin to 4 and choose the sequences of the same person or different person under different cameras as the positive or negative pairs respectively. For the fairness of experiments,

Table 1. Performance comparison of two-stream networks.

Dataset	iLIDS-VID				
	Streams	R=1	R=5	R=10	R=20
MaxPool + MaxPool		65.1	88.1	95.6	98.4
AverPool + AverPool		63.2	87.2	95.1	97.5
2 stride + 2 stride		62.5	85.4	93.6	96.3
DilatedMax + DilatedMax		64.5	87.2	95.3	97.8
MaxPool + AverPool		65.6	88.9	95.4	98.6
MaxPool + 2 stride		65.3	88.2	95.8	98.6
MaxPool + DilatedMax		65.4	88.1	95.4	98.7
AverPool + 2 stride		64.1	87.6	95.2	97.7
AverPool + DilatedMax		64.8	88.1	95.6	98.1
2 stride + DilatedMax		64.6	87.6	95.1	97.6

we set the length of each person sequence to 16 for training and 128 for testing. We set the initial learning rate to  $2e-3$ , and multiply it by 0.5 after the 800th epoch, and accomplish the training process at 1200th epoch. Given 150 persons, training for 1200 epochs takes about one day and a half using the Nvidia K80 GPU.

### 4.2. Performance evaluation of multi-streams

Before comparing the performance with the state-of-the-art methods, we conduct several experiments on iLIDS-VID dataset to verify the effectiveness of our proposed multi-stream networks.

#### 4.2.1 Networks with different streams vs. networks with same streams

To show the effectiveness of multi-stream networks, we construct two types of multi-stream architectures: networks with different streams and networks with same streams. As mentioned above, we can generate a different stream by utilizing any method such as max-pooling, average-pooling, convolutional layer with 2 stride, dilated max/average-pooling, adaptive max/average-pooling, fractional max-pooling, “upconvolutional” layer, multi-scale and upsampling. For simplicity, here we use two-stream networks to test the effectiveness of multi-stream networks. Therefore, we can get the networks with different streams by using any two generating ways. To construct the networks with same streams, we use any one of the generating ways to obtain two same sub-networks. For comparing, one of the stream for these two multi-stream architectures is identical.

The average accuracy of the comparison for these two types of multi-stream architectures is reported in Table 1. Because of large results of the combination for any two generating ways, we only test some common generating ways. It is sufficient to illustrate this phenomenon: networks with different streams work better than networks with same streams among the testing architectures. As shown in

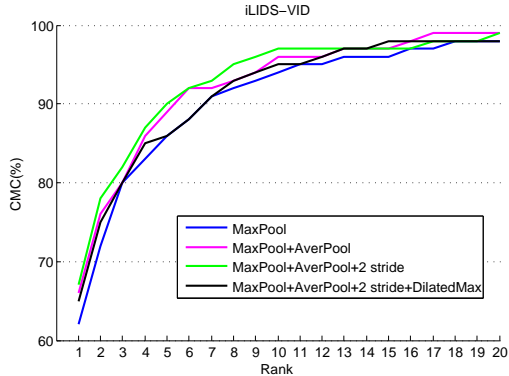


Figure 6. Performance comparison with different number of stream.

the table, the architecture with two same max-pooling sub-networks gets the best result among the testing networks with same streams. The architecture constructed with two same 2 stride sub-networks obtains the worst performance. However, when we use both max-pooling and convolutional layer with 2 stride to construct a network with different streams, we can obtain very good results. It means that a stream with the poor performance can further improve the performance of the one with good result. In other words, different streams complement each other to learn some different aspects of the feature maps, that they can not learn independently.

#### 4.2.2 Which is the best number of streams?

We construct four networks with increasing the number of streams from 1 to 4. We use the network of [35] as the one-stream architecture. The two-stream architecture is composed of max-pooling and average-pooling. We add the convolutional layer with 2 stride into two-stream network to form the three-stream architecture and the four-stream architecture consists of max-pooling, average-pooling, convolutional layer with 2 stride and dilated max-pooling. As shown in Fig. 6, the three-stream architecture gets the best performance, this is why we refer our proposed multi-stream networks as three-stream convolutional network.

#### 4.2.3 How and where to fuse multi-stream networks?

We investigate how and where to fuse multi-stream networks. The three-stream baseline architecture is used as the testing model in this part (See Fig. 2 for details). As the fusion layer can be injected at any location and two or more fusion layers can be adopted in a three-stream network, the combination of them has many options. For example, with two fusion layers, we can first fuse two streams at a certain layer and then merge with the third one at another layer. The combination of two streams has 3 situations and the

Table 2. Performance comparison for different fusion methods. The results are tested on the baseline model as shown in Fig. 2.

Dataset	iLIDS-VID			
	R=1	R=5	R=10	R=20
Sum	62.6	85.2	94.7	96.8
Max	64.7	86.6	94.8	97.3
Channel	65.4	87.8	95.3	97.4
Width	66.5	89.5	96.6	98.2
Height	66.1	88.9	96.2	97.8

Table 3. Performance comparison for Conv fusion at different fusion layers. The results are also tested on the baseline model with width fusion.

Dataset	iLIDS-VID			
	R=1	R=5	R=10	R=20
Conv1	62.3	86.4	94.8	96.7
Conv2	65.7	88.5	96.1	97.8
Conv3	66.5	89.5	96.6	98.2
Conv4	61.4	84.3	93.8	96.1

first fusion layer can be located at any layer. As a result, for a 3 layers network, it has at least 6 combinations. Hence, we only consider that one fusion layer is used in the three-stream network.

To choose the best method of fusing layers among multi-stream networks, we compare different fusion strategies with the three-stream baseline architecture. Table 2 reports the performance for all the fusion methods as described in Section 3.2. We observe that width fusion performs the best and is slightly better than height fusion. We also see that the sum fusion gets the worst result. It is not surprising as the sum fusion adds three streams together. As width fusion obtains the best performance, we use it for testing and compare the performance for fusion from different layers in Table 3. As shown in this table, fusing the three-stream network at Conv3 achieves the best performance.

### 4.3. Comparison with State-of-the-Art Methods

To further evaluate the performance of multi-stream networks, we compare the proposed three architectures with the state-of-the-art methods on iLIDS-VID, PRID-2011 and MARS datasets.

#### 4.3.1 Results on iLIDS-VID and PRID-2011

We now compare the performance of our proposed models with the state-of-the-art methods for video-based re-identification: STA [21], DVR [29], SRID [10], AFDA [13], DVDL [9], CNN-RNN [24], CNN-BRNN, ASTPN [37] and AMOC [20]. Note that the better results of AMOC are obtained by using a better optical flow algorithm [26]. With the old algorithm [22], our proposed models achieve the

Table 4. Comparison of our approaches with other state-of-the-art methods on iLIDS-VID and PRID-2011. Note that the better results of AMOC are obtained by using a better optical flow algorithm [26]. With the old algorithm [22], our proposed models achieve the best performance against all the methods including AMOC.

Dataset		iLIDS-VID				PRID-2011			
Methods	Years	R=1	R=5	R=10	R=20	R=1	R=5	R=10	R=20
STA [21]	2015	44.3	71.7	83.7	91.7	64.1	87.3	89.9	92.0
DVR [29]	2014	39.5	61.1	71.7	81.8	40.0	71.7	84.5	92.2
SRID [10]	2015	24.9	44.5	55.6	66.2	35.1	59.4	69.8	79.7
AFDA [13]	2015	37.5	62.7	73.0	81.8	43.0	72.7	84.6	91.9
DVDL [9]	2015	25.9	48.2	57.3	68.9	40.6	69.7	77.8	85.6
CNN-RNN [24]	2016	58.0	84.0	91.0	96.0	70.0	90.0	95.0	97.0
CNN-BRNN [37]	2017	55.3	85.0	91.7	95.1	72.8	92.0	95.1	97.6
ASTPN [35]	2017	62.0	86.0	94.0	98.0	77.0	95.0	99.0	99.0
AMOC + EpicFlow [20]	2017	68.7	94.3	98.3	99.3	83.7	98.3	99.4	100
AMOC + LK-Flow [20]	2017	65.3	87.3	96.1	98.4	78.0	97.2	99.1	99.7
our TSCN	-	66.5	89.5	96.6	98.2	79.2	97.4	99.5	100
our Multi-TSCN	-	67.5	90.4	97.2	98.6	78.8	96.7	99.1	99.6
Multi-Two-SCN	-	65.4	87.8	96.2	97.5	79.7	97.5	99.2	99.9

Table 5. The CMC Rank accuracy on MARS (%).

Dataset	MARS			
	R=1	R=5	R=10	R=20
RNN-CNN [24]	40.0	64.0	70.0	77.0
ASTPN [35]	44.0	70.0	74.0	81.0
Ours	45.6	72.4	75.4	82.6

best performance against all the methods including AMOC on both iLIDS-VID and PRID-2011 datasets.

The CMC results of our architectures with other models are listed in Table 4. In general, networks with different multi-streams perform better than other networks without this architecture on both iLIDS-VID and PRID-2011 datasets. With old algorithm of optical flow, our proposed two-stream multi-scale model can achieve a matching rate of rank-1 of about 65.4% on iLIDS-VID dataset, which is higher than all the testing methods. When we use three-stream multi-scale architecture, the performance can be further improved, especially for rank-1 and rank-5. The improvements are 2.1% and 2.6% for rank-1 and rank-5 respectively. For PRID-2011 dataset, the two-stream multi-scale network outperforms other methods, with rank-1 accuracy of 79.7%. It is possible that the two-stream multi-scale network has less parameters and can be trained well on the less challenging dataset. The reason that our proposed models achieve such good performance is that different multi-streams focus on different aspects of the feature maps and they complement each other to learn some union characteristics.

### 4.3.2 Results on MARS

To further evaluate the proposed architectures, we also conduct experiments on the large and realistic MARS dataset. We use the similar protocol in [35] and randomly choose two cameras of the same person for testing. Table 5 presents the performances of our model compared with the RNN-CNN and ASTPN [35]. As shown in Table 5, our proposed model still achieves the best accuracy. It again illustrates the effectiveness of our proposed architecture that uses different streams to take full use of feature maps. It should be pointed out that we only test the two-stream multi-scale architecture with max-pooling and dilated max-pooling for this dataset.

## 5. Conclusion

In this paper, we proposed a multi-stream architecture, which first uses different streams to learn different aspects of the feature maps, and then merges them together to obtain some union characteristics that can not be learned independently. Based on this architecture, we constructed a new model termed Three-Stream Convolutional Networks (TSCN), which can make full use of the learned feature maps. To further reuse the feature maps, we proposed two multi-scale architectures with the strategies of multi-scale and upsampling. We investigated the function of different streams, the methods and layers of fusion, the number of stream. Our results suggest the importance of learning correspondences between different streams. We also showed that a full connection layer in the multi-stream networks is not necessary. The comprehensive experiments indicate that our proposed networks can achieve the performance superior to the existing state-of-the-art models on iLIDS-VID,



PRID-2011 and MARS datasets. As a multi-stream architecture will generate multi-vectors, how to use outer product to obtain an efficient feature representation would be an interesting extension in further studies.

## References

- [1] D. Cheng, Y. Gong, S. Zhou, J. Wang, and N. Zheng. Person re-identification by multi-channel parts-based cnn with improved triplet loss function. In *Proceedings of the IEEE Conference on Computer Vision and Pattern Recognition*, pages 1335–1344, 2016. **1**
- [2] M. Farenzena, L. Bazzani, A. Perina, V. Murino, and M. Cristani. Person re-identification by symmetry-driven accumulation of local features. In *Proceedings of the IEEE Conference on Computer Vision and Pattern Recognition*, pages 2360–2367. IEEE, 2010. **2**
- [3] C. Feichtenhofer, A. Pinz, and A. Zisserman. Convolutional two-stream network fusion for video action recognition. In *Proceedings of the IEEE Conference on Computer Vision and Pattern Recognition*, pages 1933–1941, 2016. **1**
- [4] D. Gray, S. Brennan, and H. Tao. Evaluating appearance models for recognition, reacquisition, and tracking. In *Proc. IEEE International Workshop on Performance Evaluation for Tracking and Surveillance (PETS)*, volume 3, pages 1–7. Citeseer, 2007. **1**
- [5] D. Gray and H. Tao. Viewpoint invariant pedestrian recognition with an ensemble of localized features. In *European Conference on Computer Vision*, pages 262–275. Springer, 2008. **2**
- [6] K. He, X. Zhang, S. Ren, and J. Sun. Deep residual learning for image recognition. In *Proceedings of the IEEE Conference on Computer Vision and Pattern Recognition*, pages 770–778, 2016. **1**
- [7] M. Hirzer, C. Beleznaï, P. M. Roth, and H. Bischof. Person re-identification by descriptive and discriminative classification. In *Scandinavian Conference on Image Analysis*, pages 91–102. Springer, 2011. **6**
- [8] S. Karaman and A. D. Bagdanov. Identity inference: generalizing person re-identification scenarios. In *European Conference on Computer Vision*, pages 443–452. Springer, 2012. **3**
- [9] S. Karanam, Y. Li, and R. J. Radke. Person re-identification with discriminatively trained viewpoint invariant dictionaries. In *Proceedings of the IEEE International Conference on Computer Vision*, pages 4516–4524, 2015. **7, 8**
- [10] S. Karanam, Y. Li, and R. J. Radke. Sparse re-id: Block sparsity for person re-identification. In *Proceedings of the IEEE Conference on Computer Vision and Pattern Recognition Workshops*, pages 33–40, 2015. **7, 8**
- [11] A. Klaser, M. Marszałek, and C. Schmid. A spatio-temporal descriptor based on 3d-gradients. In *British Machine Vision Conference*, 2008. **3**
- [12] I. Kviatkovsky, A. Adam, and E. Rivlin. Color invariants for person re-identification. *IEEE Transactions on Pattern Analysis and Machine Intelligence*, 35(7):1622–1634, 2013. **2**
- [13] Y. Li, Z. Wu, S. Karanam, and R. J. Radke. Multi-shot human re-identification using adaptive fisher discriminant analysis. In *British Machine Vision Conference*, 2015. **7, 8**
- [14] Y. Li, Z. Ye, and J. M. Rehg. Delving into egocentric actions. In *Proceedings of the IEEE Conference on Computer Vision and Pattern Recognition*, pages 287–295, 2015. **1**
- [15] Z. Li, S. Chang, F. Liang, T. S. Huang, L. Cao, and J. R. Smith. Learning locally-adaptive decision functions for person verification. In *Proceedings of the IEEE Conference on Computer Vision and Pattern Recognition*, pages 3610–3617, 2013. **1**
- [16] S. Liao, Y. Hu, X. Zhu, and S. Z. Li. Person re-identification by local maximal occurrence representation and metric learning. In *Proceedings of the IEEE Conference on Computer Vision and Pattern Recognition*, pages 2197–2206, 2015. **2**
- [17] S. Liao and S. Z. Li. Efficient psd constrained asymmetric metric learning for person re-identification. In *Proceedings of the IEEE International Conference on Computer Vision*, pages 3685–3693, 2015. **2**
- [18] C. Liu, S. Gong, C. C. Loy, and X. Lin. Person re-identification: What features are important? In *European Conference on Computer Vision*, pages 391–401. Springer, 2012. **2**
- [19] H. Liu, J. Feng, M. Qi, J. Jiang, and S. Yan. End-to-end comparative attention networks for person re-identification. *IEEE Transactions on Image Processing*, 2017. **1**
- [20] H. Liu, Z. Jie, K. Jayashree, M. Qi, J. Jiang, S. Yan, and J. Feng. Video-based person re-identification with accumulative motion context. *arXiv preprint arXiv:1701.00193*, 2017. **1, 3, 7, 8**
- [21] K. Liu, B. Ma, W. Zhang, and R. Huang. A spatio-temporal appearance representation for video-based pedestrian re-identification. In *Proceedings of the IEEE International Conference on Computer Vision*, pages 3810–3818, 2015. **7, 8**
- [22] B. D. Lucas, T. Kanade, et al. An iterative image registration technique with an application to stereo vision. pages 674–679. Vancouver, BC, Canada, 1981. **7, 8**
- [23] B. Ma, Y. Su, and F. Jurie. Local descriptors encoded by fisher vectors for person re-identification. In *Computer Vision—ECCV 2012. Workshops and Demonstrations*, pages 413–422. Springer, 2012. **2**
- [24] N. McLaughlin, J. Martinez del Rincon, and P. Miller. Recurrent convolutional network for video-based person re-identification. In *Proceedings of the IEEE Conference on Computer Vision and Pattern Recognition*, pages 1325–1334, 2016. **1, 3, 5, 7, 8**
- [25] S. Paisitkriangkrai, C. Shen, and A. van den Hengel. Learning to rank in person re-identification with metric ensembles. In *Proceedings of the IEEE Conference on Computer Vision and Pattern Recognition*, pages 1846–1855, 2015. **2**
- [26] J. Revaud, P. Weinzaepfel, Z. Harchaoui, and C. Schmid. Epicflow: Edge-preserving interpolation of correspondences for optical flow. In *Proceedings of the IEEE Conference on Computer Vision and Pattern Recognition*, pages 1164–1172, 2015. **7, 8**

- [27] K. Simonyan and A. Zisserman. Two-stream convolutional networks for action recognition in videos. In *Advances in Neural Information Processing Systems*, pages 568–576, 2014. [1](#)
- [28] F. Wang, W. Zuo, L. Lin, D. Zhang, and L. Zhang. Joint learning of single-image and cross-image representations for person re-identification. In *Proceedings of the IEEE Conference on Computer Vision and Pattern Recognition*, pages 1288–1296, 2016. [1](#)
- [29] T. Wang, S. Gong, X. Zhu, and S. Wang. Person re-identification by video ranking. In *European Conference on Computer Vision*, pages 688–703. Springer, 2014. [6](#), [7](#), [8](#)
- [30] K. Q. Weinberger and L. K. Saul. Distance metric learning for large margin nearest neighbor classification. *Journal of Machine Learning Research*, 10(Feb):207–244, 2009. [2](#)
- [31] L. Wu, C. Shen, and A. v. d. Hengel. Personnet: Person re-identification with deep convolutional neural networks. *arXiv preprint arXiv:1601.07255*, 2016. [1](#), [3](#)
- [32] T. Xiao, H. Li, W. Ouyang, and X. Wang. Learning deep feature representations with domain guided dropout for person re-identification. In *Proceedings of the IEEE Conference on Computer Vision and Pattern Recognition*, pages 1249–1258, 2016. [1](#)
- [33] T. Xiao, S. Li, B. Wang, L. Lin, and X. Wang. End-to-end deep learning for person search. *arXiv preprint arXiv:1604.01850*, 2016. [1](#)
- [34] F. Xiong, M. Gou, O. Camps, and M. Szaier. Person re-identification using kernel-based metric learning methods. In *European Conference on Computer Vision*, pages 1–16. Springer, 2014. [2](#)
- [35] S. Xu, Y. Cheng, K. Gu, Y. Yang, S. Chang, and P. Zhou. Jointly attentive spatial-temporal pooling networks for video-based person re-identification. *arXiv preprint arXiv:1708.02286*, 2017. [1](#), [5](#), [6](#), [7](#), [8](#)
- [36] Y. Yan, B. Ni, Z. Song, C. Ma, Y. Yan, and X. Yang. Person re-identification via recurrent feature aggregation. In *European Conference on Computer Vision*, pages 701–716. Springer, 2016. [3](#)
- [37] W. Zhang, X. Yu, and X. He. Learning bidirectional temporal cues for video-based person re-identification. *IEEE Transactions on Circuits and Systems for Video Technology*, 2017. [1](#), [3](#), [7](#), [8](#)
- [38] Z. Zhang, Y. Chen, and V. Saligrama. Group membership prediction. In *Proceedings of the IEEE International Conference on Computer Vision*, pages 3916–3924, 2015. [2](#)
- [39] R. Zhao, W. Ouyang, and X. Wang. Person re-identification by saliency matching. In *Proceedings of the IEEE International Conference on Computer Vision*, pages 2528–2535, 2013. [2](#)
- [40] R. Zhao, W. Ouyang, and X. Wang. Learning mid-level filters for person re-identification. In *Proceedings of the IEEE Conference on Computer Vision and Pattern Recognition*, pages 144–151, 2014. [2](#)
- [41] L. Zheng, Z. Bie, Y. Sun, J. Wang, C. Su, S. Wang, and Q. Tian. Mars: A video benchmark for large-scale person re-identification. In *European Conference on Computer Vision*, pages 868–884. Springer, 2016. [6](#)
- [42] W.-S. Zheng, S. Gong, and T. Xiang. Reidentification by relative distance comparison. *IEEE Transactions on Pattern Analysis and Machine Intelligence*, 35(3):653–668, 2013. [2](#)
- [43] Z. Zhou, Y. Huang, W. Wang, L. Wang, and T. Tan. See the forest for the trees: Joint spatial and temporal recurrent neural networks for video-based person re-identification. In *Proceedings of the IEEE Conference on Computer Vision and Pattern Recognition*, pages 4747–4756, 2017. [3](#)